Mesh2Measure: A Novel Body Dimensions Measurement Based on 3D Human Model

Tao Song(✉), Rui Zhang, Yukun Dong, Xixi Tao, Hongcui Lu, and Baohua Liu

China University of Petroleum (East China), Qingdao 266580, China
{tsong,dongyk}@upc.edu.cn

Abstract. In this work, we propose an anthropometric dimensions measurement method based on 3D human model, namely Mesh2Measure. In our method, Human body features in the front and side images are firstly extracted and fused. And then, the feature vectors are attached to the template mesh model SMPL by using Graph-CNN, and 3D coordinates of the model vertices are regressed. Anthropometric dimensions of height, length, width and depth are calculated by scale conversion based on the model vertex coordinates. A novel general dense elliptic model is developed for the curve dimension or closed circumference dimension, which obtains human body dimensions by accumulating the length of elliptic segments with different coefficients. Data experiments are conducted by measuring 100 subjects. Experimental results show that our Mesh2Measure model can measure 38 main dimensions of human body in 15 s, and more importantly, the accuracy rate is 97.4% compared with the ground truth dimensions by manual measurements.

Keywords: Anthropometric dimensions · 3D Human reconstruction · Dense elliptic model

1 Introduction

Anthropometry is a branch of anthropology, focusing on anthropometrics and observation methods, and exploring the characteristics, types, variation and development of the human body through measurements of human body. Under the framework of industry 5.0, remote acquisition of anthropometric dimensions is of great significance to theoretical research of anthropology. It also has vital applications in medical care, forensic anthropology, sports, monitoring, garment customization and other fields. In health care, for example, it can help detect potential health problems in people. For instance, abdominal obesity was associated with gastroesophageal reflux disease (GERD) and Barrett's esophagus (BE), and by abdominal diameter index, we can predict the existence of BE better than body mass index (BMI) and waist-to-hip ratio (WHR) [1]. Koning et al. [2] showed a stronger correlation between waist-to-hip ratio and cardiovascular disease, and suggested that these measurements should be included in cardiovascular risk assessment. In addition, dimensions such as cervical spine height, high hip depth, and high hip circumference can be used to detect postural disorders [3]. According to the waist depth

Z. Lv and H. Song (Eds.): INTETAIN 2021, LNICST 429, pp. 80–99, 2022.
https://doi.org/10.1007/978-3-030-99188-3_6

data, we can analyze the metabolic triad of atherosclerosis [4], and waist circumference can be used to analyze obesity and lung function [5]. In health care, the risk of heart disease and premature death can be estimated by thigh circumference [6]. Using chest circumference data can detect the risk of coronary heart disease [7]. Hip circumference can be used to measure pelvic tilt an d analyze the incidence rate and mortality of cardiovascular diseases [8]. It is obtained in [9] that people with too small calf circumference are prone to carotid plaque and atherosclerosis, leading to myocardial infarction and stroke, and the probability of insulin resistance increases, leading to diabetes [10].

Traditional anthropometric dimensions measurement methods mainly adopt contact measurement. These methods are intuitive and easy to use, but their applicability is limited and affected by many other factors. Surveyors with different skills and experience levels will make different human errors, and multiple operations of one surveyor will be different. Non-contact body measurement methods based on 2D images can be found in [11, 12, 16, 18, 31]. These methods require all subjects to take the front, side images in a required posture to calculate the length, width and other dimensions of all part of the human body.

In recent years, it has become one of research directions of anthropometric measurement to obtain dimensions based on 3D human model [13–15]. There are still many problems in current methods of accurately obtaining anthropometric dimensions based on 3D human body model. Firstly, the 3D model based on single image reconstruction has inherent fuzziness in shape estimation, which cannot meet the requirements of accurate measurement. Secondly, taking linear length accumulation between points as measurement dimensions may lead measurement error. Thirdly, there is no robust method to adapt to various body types.

We propose here a novel anthropometric dimensions measurement method based on 3D human body model, namely Mesh2Measure. In our method, the typical depth convolution neural networks Resnet-50 are used to extract and fuse human features in 2D images, and then the feature vector is attached to a standard mesh model SMPL from [17]. Vertex coordinates of the reconstructed model are obtained by using GraphCNN to deform vertices of model point by point. Dimensions of model are calculated by using these vertexes coordinates and the measurement datum points. In order to improve accuracy of model to meet the requirements of our dimension measurement, we used two view images of human body in MeshNet stage to reconstruct 3D human body model. Data experiments are conducted by measuring 100 subjects. Experimental results show that our Mesh2Measure model can measure 38 main dimensions of human body in 15 s, and the accuracy rate is 97.4% compared with the ground truth dimensions.

Our contributions can be summarized as follows.

1) Mesh2Measure uses two views to reconstruct the 3D human body model. This avoids the inherent ambiguity of single-view reconstruction of the human model.
2) A dense elliptic model is proposed. The length of the elliptic segment with different coefficients is accumulated as the calculation method of the curve dimension and the closed circumference dimension to reduce the error.

2 Our Mesh2Measure Model

We design Mesh2Measure in a cascaded architecture, which consists of MeshNet and Measure. Figure 1 describes the overall architecture of the system.

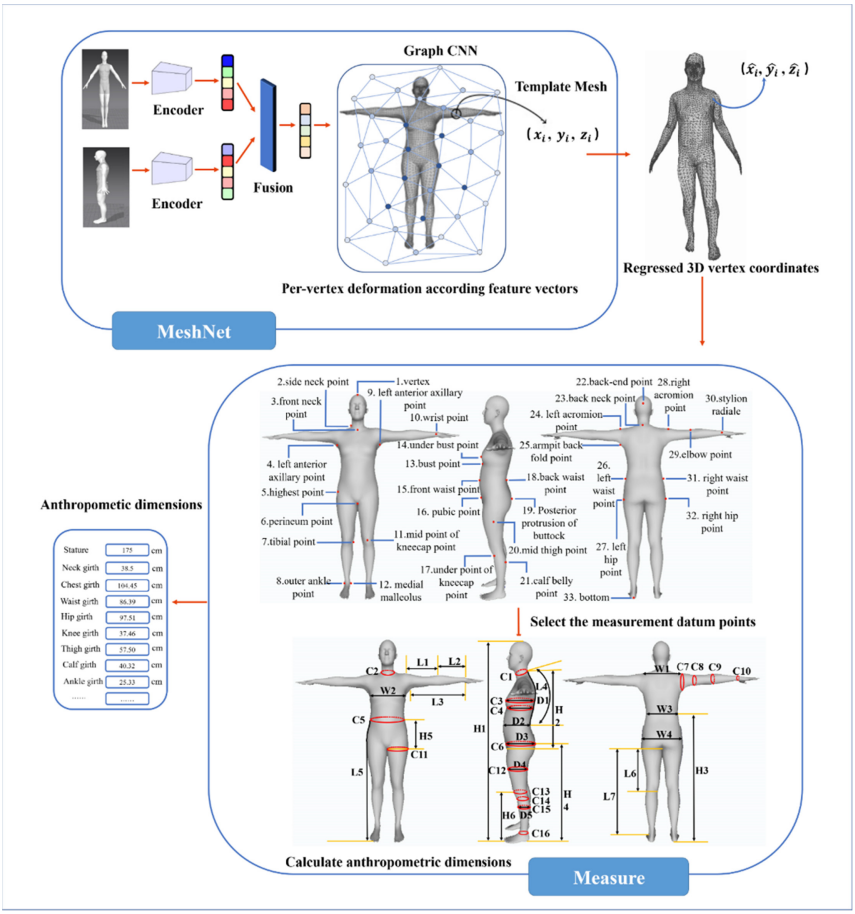

Fig. 1. Overview of Mesh2Measure framework. Given two images (front image and side image), MeshNet architecture performs 3D human body reconstruction based on the given images, and then the Measure architecture obtains human body dimensions based on the reconstructed human body model.

MeshNet is responsible for reconstructing the human body mesh model based on images from different perspectives, Measure is responsible for the selection of measurement points and the calculation of dimensions. Our Mesh2Measure can measure all the dimensions mentioned in GB/T 16160–2017 [29], and compare the main 38 dimensions of human body measured with the truth dimensions to determine that the error is within the allowable range of the tolerance standard of all dimensions of clothing, and our method is more robust to the special body type of people.

2.1 MeshNet

MeshNet architecture is mainly responsible for 3D human model reconstruction using two 2D images with architectures from [24, 27]. Human body features of two view images are extracted and fused based on Resnet-50 network to get a 2048-D feature vector. And then these features are attached to vertices of a template mesh model SMPL, using Graph-CNN deforms vertices of the mesh model point by point. Finally, MeshNet outputs vertexes coordinates of the deformed mesh model.

Feature Extraction and Fusion Network Based on Resnet-50
The first part of MeshNet architecture consists of a feature extractor, which extracts the human feature information from the image for model reconstruction. In order to reduce the error of body shape estimation by complex posture and make the network extract body shape features better, we consider separating posture feature extraction from body shape feature extraction. The accuracy of feature extraction affects the accuracy of model reconstruction. It is difficult to extract the comprehensive three-dimensional information of human body with traditional single view feature extraction. We propose here a multi view feature extraction and fusion network, which uses two view images as input. The two implementation methods of multi view feature fusion strategy is shown in Fig. 2. The fusion strategy of the former is to decouple the image features from different angles, so we use the former method to extract human features for images with different viewing angles by using separate subnets. Multiple subnets work in parallel. Finally, the feature vectors obtained from different subnets are weighted and averaged as the final feature representation. Experiments show that the two view images reconstruction model can meet our accuracy requirements.

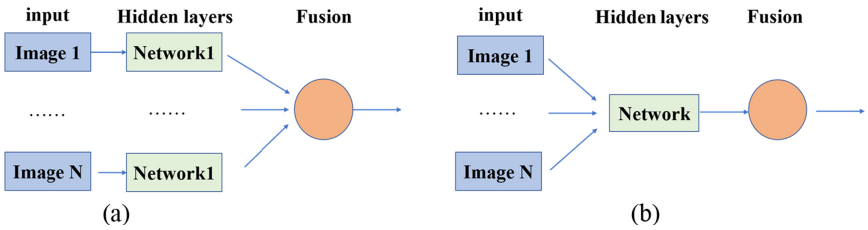

Fig. 2. Multi-view fusion strategy. (a) One view corresponds to one network strategy. (b) Multiple views correspond to one network strategy.

Our feature extraction and fusion network is composed of two ResNet-50 [27] networks trained on ImageNet. Of course, there are many other feature extraction networks, such as AlexNet [32],VGG16 [33] and GoogLeNet [34]. Based on their performance on image classification tasks, we decided to still use ResNet-50 to complete our feature extraction task. According to our requirements, the final fully connected layer of Resnet-50 network is removed, the 2048-D feature vectors output by the average pooling layer are retained, and the feature vectors extracted from different subnets are input into the feature fusion layer for weighted average fusion operation. The architecture of feature extraction and fusion network is shown in Fig. 3.

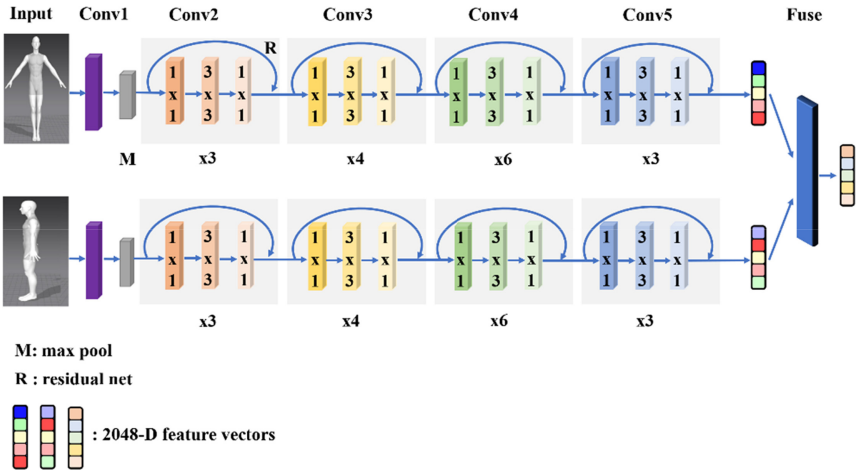

Fig. 3. The network architecture of feature extraction and fusion based on ResNet-50.

3D Human Model Reconstruction Network Based on Graph-CNN

SMPL (Skinned Multi-Person Linear Model) is a vertex-based and most widely used parameterized human body mesh model, which contains 6980 vertices, 13776 triangular patches, and a skeleton with 24 joint points. Among them, from the left to the right of the model is the positive direction of the X axis, from the bottom to the top, that is, the standing direction of the human is the positive direction of the Y axis, and the direction of the line of sight of the human eye perpendicular to the X axis and Y axis is the Z axis, as shown in Fig. 4. The SMPL parametric model includes 10 β parameters representing human body shape and 75 θ parameters representing human motion posture and joint relative angle. By modifying the pose and shape parameters, a 3D model with 3D human joints and mesh vertex coordinates can be generated. 3D human body reconstruction based on deep convolution neural network includes model-based method and model-free method. The model-based method [19–22] trains the network and estimates the SMPL parameters from the input image; the model-free [23–26] method directly estimates mesh vertex coordinates. In this paper, the model-free method is used to regress the vertex coordinates of the mesh instead of the model parameters.

The second part of MeshNet architecture is to deform the extracted human features to get the 3D coordinates of the mesh model vertices. Since our goal is to regress the vertex coordinates to meet the measurement requirements, rather than output the model parameters, we learn the method given by kolotouros et al. [24], and use Graph CNN to simplify the regression. Human features extracted from feature extraction and fusion network are added to the vertices of SMPL template mesh, and Graph-CNN is responsible for processing them on the mesh structure. The vertex coordinates after point by point deformation are output to restore the complete 3D geometry of the mesh.

Graph CNN is performed by a series of graph convolutions [28]. The formula is defined as,

$$Y = \tilde{A}XW \tag{1}$$

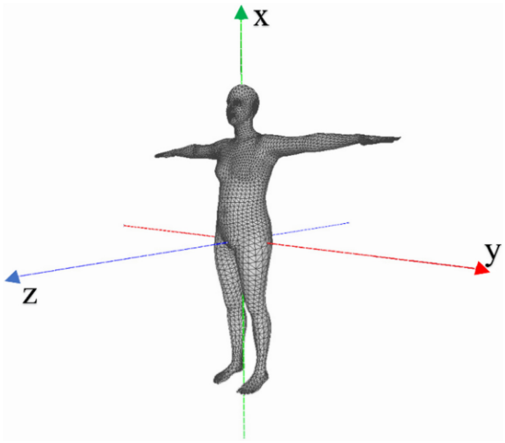

Fig. 4. SMPL model.

where A is the row normalized adjacency matrix, X is the input eigenvector, and W is the weight matrix. In this experiment, the weight data of Kolotouros training is used for regression. The full loss is defined as,

$$L = L_{joint} + L_{mesh} \tag{2}$$

$$L_{joint} = \sum_{k=1}^{M} \left\| \widehat{J_k} - J_k \right\|_1 \tag{3}$$

$$L_{mesh} = \sum_{i=1}^{N} \left\| \widehat{V_i} - V_i \right\|_1 \tag{4}$$

J_k is the ground truth 2D joints locations,$\widehat{J_k}$ is obtained by projecting 3D joint points of the predicted 3D mesh shape onto the image plane , L_{joint} is the L_1 loss of the predicted joints locations and the ground truth joints. L_{mesh} is a per-vertex L_1 loss about the predicted 3D mesh shape and the ground truth 3D mesh shape. $\widehat{V_i}$ represents our predicted 3D mesh vertices and V_i represents the ground truth of 3D mesh vertices.

2.2 Measure

As the second part of Mesh2Measure architecture, Measure mainly selects measurement datum points on the 3D human body mesh model, and calculates dimensions according to the spatial relationship between the points. We first introduce the selection basis and strategy of measurement points based on mesh model. Then, the method of dimension calculation based on the measurement datum points is introduced.

Measurement Point Selection Based on 3D Human Body Mesh Model
Whether it is contact measurement or non-contact measurement, most of them rely on measurement datum points highly related to the body parts. The measurement based on 3D human body model can make better use of 3D information of the human body, and

the effect is almost equivalent to the manual measurement on a real human body. We mark corresponding measurement datum points on the 3D model in accordance with the provisions of GB/T 38131–2019 [30] on a template mesh model, and determine corresponding dimension points near measurement datum points according to dimensions measurement definition, so as to realize the automatic measurement of all 3D human model dimensions. For example, in order to obtain the waist measurement points, first the front waist point, side waist point and back waist point are determined, then the vertices on the same horizontal line with these datum points are selected, the waist measurement points are recorded in turn, and finally the waist measurement points are obtained, as shown in Fig. 5. Figure 6 shows measurement datum points of all marks, and Table 1 shows the measurement datum points of each dimension and corresponding vertexes serial numbers on the reconstructed human model.

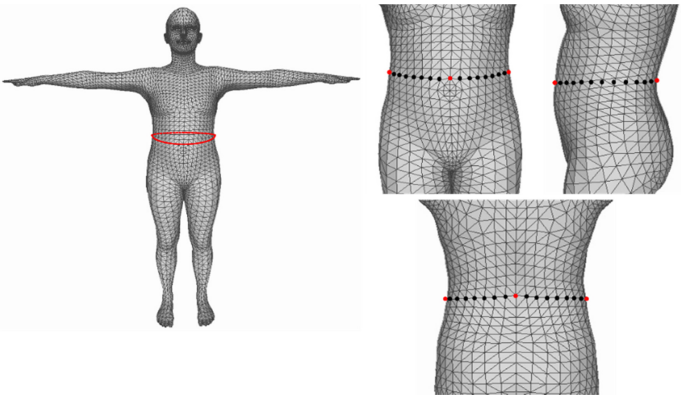

Fig. 5. Schematic diagram of waist measurement point selection.

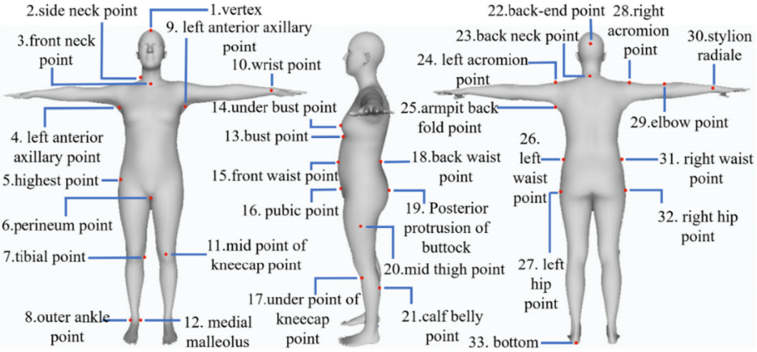

Fig. 6. The datum points of anthropometry.

Table 1. Anthropometric dimensions and characteristic points.

Classification	Body dimension	Dimension mark	Auxiliary measurement points	Corresponding vertex number on the model
Height	Stature	H1	1,33	411,3426
	Torso height	H2	6,23	1208,3164
	Waist height	H3	18,33	3502,3426
	Hip height	H4	19,33	1246,3426
	Straight body rise	H5	6,15	1208,3504
	Knee height	H6	11,33	4533,3426
Length	Upper-arm length	L1	28,29	5342,5112
	Lower-arm length	L2	29,30	5112,5568
	Under-arm length	L3	9,10	1545,2112
	Back neck point to waist	L4	18,23	3502,3164
	Outside-leg length	L5	5,31,33	4332,4310,3426
	Thigh length	L6	6,7	1208,4635
	Inside-leg length	L7	6,8	1208,6727
Width	Shoulder width	W1	24,28	3011,5342
	Chest width	W2	4,9	5013,1545
	Waist width	W3	26,31	676,4310
	Hip width	W4	27,32	1447,4920
Depth	Chest depth	D1	13	3042
	Waist depth	D2	15,18	3504,3502
	Hip depth	D3	16,19	1807,1246
	Thigh depth	D4	20	904
	Calf depth	D5	21	1183
Circumference	Neck circumference	C1	2,23	3721,3164
	Neck-base circumference	C2	2,3,23	3721,3168,3164

(*continued*)

Table 1. (*continued*)

Classification	Body dimension	Dimension mark	Auxiliary measurement points	Corresponding vertex number on the model
	Chest circumference	C3	4,9,13	5013, 1545, 3042
	Under-chest circumference	C4	14	1329
	Waist circumference	C5	15,18,26,31	3504, 3502, 676, 4310
	Hip circumference	C6	19,27,32	1246, 1447, 4920
	Armscye circumference	C7	24,25	3011,1879
	Upper-arm circumference	C8	28,29	5342, 5112
	Elbow circumference	C9	29	5112
	Wrist circumference	C10	20,30	904, 5568
	Thigh circumference	C11	6	1208
	Mid-thigh circumference	C12	20	904
	Knee circumference	C13	11	4533
	Under-knee circumference	C14	17	1073
	Calf circumference	C15	21	1183
	Ankle circumference	C16	8,12	6727,6833

Calculation of Anthropometric Dimensions Based on Dense Elliptic Model

Based on the measurement point list of the model, we calculated 38 main dimensions of human body, including 6 height dimensions, 7 length dimensions, 4 width dimensions, 5 thickness dimensions and 16 circumference dimensions, as shown in Fig. 7. Once the real height of the subject is known, the ratio of the real height to the model height is used as the conversion scale of dimensions of other parts.

It needs to calculate the coordinate difference or vector length of several measurement feature points in a certain direction according to the human body measurement points. For special arc lengths such as L4 and H1, they are composed of several small arc

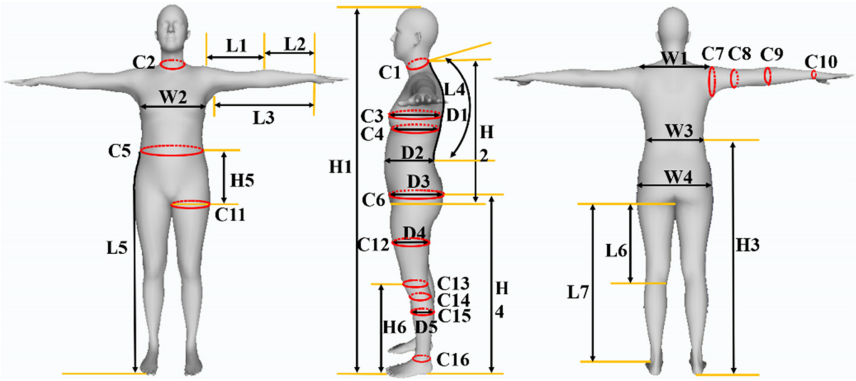

Fig. 7. Anthropometric dimensions obtained from 3D human model.

lengths. The length of each arc is approximated by its inscribed chord, and the length of the whole arc can be regarded as the sum of the lengths of several inscribed chords. We take the enclosed circumference as the result of the stitching of elliptic curve segments with different ellipse coefficients, and propose a dense elliptic model. In other words, the measurement points corresponding to the enclosed circumference dimension are projected towards a certain direction to obtain the corresponding two-dimensional curve. The two-dimensional curve can be regarded as composed of elliptic segments with different elliptic coefficients, and the calculated circumference dimension is obtained by accumulating the lengths of multiple elliptic curve segments, as shown in Fig. 8 (a).

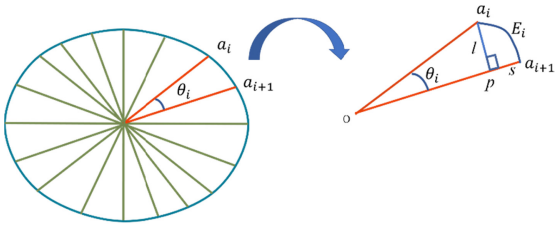

Fig. 8. Closed curve size fitting diagram.

As shown in Fig. 8 (b), given the centre point O and coordinates of the point sequence constituting the closed curve, a_i and a_{i+1} are the boundary points of the elliptic segment, Oa_i and Oa_{i+1} are the length of the edge, and the included angle θ_i can be calculated by the line segments Oa_i and Oa_{i+1}. The point P can be obtained by taking the endpoint of the relatively short side of Oa_i and Oa_{i+1} as a vertical line to the longer side, and the lengths of OP, Pa_i and Pa_{i+1} can be obtained respectively. Taking P as the coordinate origin, the relatively long side of Pa_i and Pa_{i+1} as the long half axis l and the short side as the short half axis s, the elliptic equation L is established, and the arc length E_i is one

fourth of the circumference of the elliptic. The formula is defined as follows,

$$C_{L_i} = 2\pi s_i + 4(l_i - s_i) \tag{5}$$

$$E_i = \frac{1}{4} C_{L_i} \tag{6}$$

The elliptic segments composed of different elliptic coefficients are accumulated to obtain closure circumference dimensions, where E_{all} represents the dimension to be measured, N represents the number of angles corresponding to each elliptic segment, and E_N represents the length of the elliptic segment composed of vertices a_N and a_1.

$$E_{all} = \sum_{i=1}^{N-1} \frac{1}{4}[2\pi s_i + 4(l_i - s_i)] + E_N \tag{7}$$

3 Results and Discussion

3.1 Datasets

Human3.6M: This is an indoor shot 3D pose dataset that contains 11 professional actors (6 male, 5 female) in 17 scenarios like smoking, taking photo, taking on the phone, eating. Based on our needs, we selected pictures from two perspectives of a subject in different scenarios. In order to improve the robustness of the model, the selected angles are not strict front and side photos. The data sets selected from S5, S7, S8 and S9 are used for training, and the data sets selected from S10 and S11 are used for testing.

Human-Measure: We collected a data set including the front and side images, and anthropometric dimensions to test our proposed algorithm. These data are from 100 volunteers, as shown in Table 2, including 52 females and 48 males, aged between 20 and 55 years old, and include a wealth of body types. People in the images are all dressed in tight clothes and stand in an upright position so that the outline of the body can be clearly seen. Figure 9 shows the scatter plots of age and BMI distribution of subjects in the data set.

Table 2. Dataset parameters.

Number of volunteers	Sex	Age	Weight(kg)	Body mass index
52	Female	19–76	42–92	18.3–33.3
48	Male	18–72	53–103	17.4–32.6

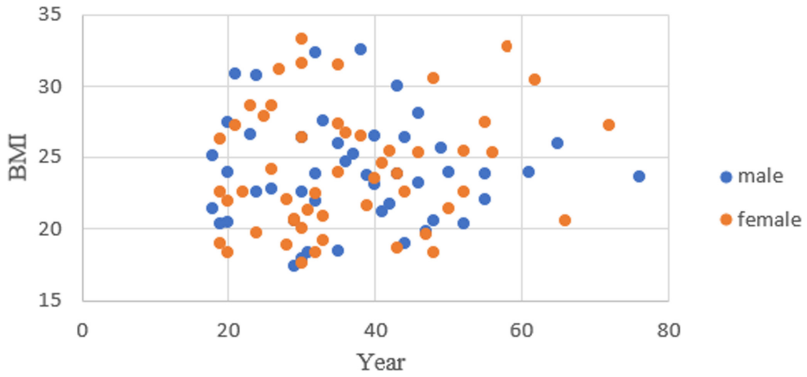

Fig. 9. Scatter plot of age and body mass index distribution of the data sets we collected.

3.2 Experimental Results

We used reconstruction error and MPJPE [38] to evaluate the pose reconstruction result of our model on Human3.6M. Table 3 showed the comparison of our method with other excellent 3D reconstruction methods, and the data of different methods are the best results they report. Our method is better than the optimized baseline, which shows that our improved method has a clear improvement on the effect of reconstruction.

According to dimensions definition and method requirements of clothing specific anthropometry, three experienced surveyors measured the actual dimension of 100 volunteers for two consecutive days and calculated the average dimension G_k as the truth value of the dimension. During the measurement, the subjects should wear tight clothes to avoid the clothing affecting the human body shape or hindering the accuracy of the dimension. The height of the human body is measured with a human altimeter, and all horizontal and other dimensions are measured with a tape. The tape should be properly tightened and the human body should not be oppressed by the tape.

$$G_k = \frac{1}{a}\left(\sum_{i=0}^{a}\left(\frac{1}{c}\sum_{j=1}^{c} m_{ij}\right)\right) \tag{8}$$

Table 3. Comparison with other methods on Human3.6M (Protocol 2[19]).

Method	MPJPE (mm)	Reconstruction error (mm)
Lassner et al. [36]	-	93.9
SMPLify [35]	-	82.3
Pavlakos et al. [20]	-	75.9
NBF [37]	-	59.9
HMR [19]	87.97	56.8
CMR [24]	102.1	50.1
Ours	100.87	48.9

Here, G_k represents true value of the kth dimension, a represents the number of surveyors, c is the number of measurements, and m_{ij} represents the jth measurement value of the ith surveyor. There are inevitably two kinds of errors in face-to-face manual measurement, one is the inter-observer error when different surveyors measure the same dimension, the other is the intra-observer error caused by multiple measurements of a certain dimension by the same surveyor. In order to evaluate the influence of these two manual measurement errors on our experimental results, the measurement technical error (TEM) and reliability coefficient (R) of 100 volunteers were calculated for each dimension, and the formula was defined as follows,

$$TEM = \frac{\sum_1^n \left[\left(\sum_1^a m_a^2 \right) - \left(\left(\sum_1^a m_a^2 \right) / a \right) \right]}{n(a-1)} \tag{9}$$

$$R = 1 - \left(\frac{TEM^2}{S^2} \right) \tag{10}$$

In the above formula, n is the number of volunteers to be measured, a is the number of measurement personnel to perform the measurement, when calculating the first type of intra-observer error, the number of measurements is a, when calculating the second type of inter-observer error, the number of measurements is 2a. Therefore, in this experiment, each surveyor needs to make two measurements. s^2 is the sample variance. The results of the calculated intra-observer and inter-observer reliability coefficients are shown in Table 4.

Table 4. Reliability of manually measured dimensions.

Dimension	Inter-observer reliability	Intra-observer reliability		
	R	Surveyor1	Surveyor2	Surveyor3
H1	0.87	0.91	0.96	0.94
H2	0.84	0.88	0.89	0.86
H3	0.86	0.85	0.93	0.89
H4	0.82	0.83	0.89	0.91
H5	0.81	0.86	0.94	0.96
H6	0.84	0.94	0.98	0.98
L1	0.90	0.87	0.91	0.84
L2	0.92	0.85	0.96	0.92
L3	0.78	0.84	0.84	0.81
L4	0.83	0.89	0.91	0.93
L5	0.87	0.91	0.96	0.83
L6	0.83	0.89	0.9	0.92

(*continued*)

Table 4. (*continued*)

Dimension	Inter-observer reliability	Intra-observer reliability		
	R	Surveyor1	Surveyor2	Surveyor3
L7	0.89	0.90	0.93	0.89
W1	0.82	0.93	0.86	0.93
W2	0.79	0.88	0.97	0.87
W3	0.88	0.87	0.90	0.98
W4	0.94	0.82	0.96	0.92
D1	0.94	0.96	0.93	0.96
D2	0.85	0.92	0.87	0.89
D3	0.96	0.90	0.93	0.87
D4	0.92	0.95	0.86	0.93
D5	0.79	0.86	0.90	0.75
C1	0.93	0.88	0.88	0.85
C2	0.87	0.89	0.90	0.93
C3	0.85	0.85	0.89	0.86
C4	0.83	0.98	0.92	0.95
C5	0.91	0.86	0.97	0.87
C6	0.90	0.96	0.94	0.93
C7	0.89	0.94	0.85	0.94
C8	0.88	0.96	0.89	0.95
C9	0.94	0.85	0.92	0.91
C10	0.81	0.82	0.85	0.83
C11	0.76	0.83	0.96	0.89
C12	0.85	0.88	0.89	0.95
C13	0.86	0.94	0.93	0.91
C14	0.84	0.92	0.95	0.94
C15	0.95	0.85	0.84	0.79
C16	0.82	0.86	0.91	0.98

As shown in Table 4, after calculation, the average value of inter-observer reliability is 0.864 (range: 0.75–0.96), which shows good reliability. In addition, the mean intra-observer reliability of the three measurers are 0.889 (range: 0.83–0.98), 0.912 (range: 0.84–0.98) and 0.901 (range: 0.78–0.98). From the calculation results, it can be seen that the human body dimensions measured manually is reliable and within the allowable measurement error range.

Next, we evaluate our Mesh2Measure measurement method. The measurement values obtained by our method are affected by two factors: (1) the degree of relaxation of the subject's clothes and the complexity of the background lead to the inaccurate display of the body shape, which affects the estimation of the body shape, resulting in the generation of size measurement errors. (2) the distance between the camera and the subject. These factors should be adjusted in the test process to obtain more favorable measurement results. The measurement error of a dimension is absolute difference between dimension obtained by our method and measured manually dimension. The mean absolute difference (MAD) between dimension obtained automatically and dimension measured manually is taken as the accuracy evaluation standard of our method. MAD of the kth dimension is defined as,

$$MAD_k = \frac{1}{n}\sum_{i=1}^{n} |M_i - G_i| \tag{11}$$

Among them, M_i is the dimension of the ith subject measured by our method, G_i is the average size of volunteers measured by all surveyors, and N is the number of volunteers.

In this paper, 38 main dimensions of 100 volunteers were evaluated. Firstly, three-dimensional human models were reconstructed based on single image, dual image and three images respectively, and the dimensions were measured on the models. The curve dimension and circumference dimension were calculated by point-to-point linear distance accumulation method, and the MAD values were MAD-1-pp and MAD-2-pp, MAD-3-pp. In addition, we use the dense ellipse model to calculate the curve dimension and circumference dimension based on the 3D model reconstructed from double image to evaluate the accuracy of our dense ellipse model, and the MAD value was expressed by MAD-2-e, as shown in Table 5.

Table 5. Comparison table of human body size measurement accuracy.

Classification	Dimension mark	MAD-1-pp(mm)	MAD-2-pp(mm)	MAD-3-pp(mm)	MAD-2-e(mm)	MAE
Height	H1	3.4	3.4	3.4	3.4	6
	H2	4.5	4.4	4.4	4.4	×
	H3	5	4.8	4.8	4.8	7
	H4	5.8	5.5	5.5	5.5	×
	H5	6.8	6.5	6.5	6.5	×
	H6	2.1	2	2	2	3
Length	L1	2.6	2.6	2.7	2.6	6
	L2	4.3	4.3	4.3	4.3	6
	L3	4.4	4.3	4.3	4.3	6
	L4	6.2	5.9	5.9	4.7	×
	L5	5.3	5.3	5.3	5	×
	L6	6.5	6.1	6.1	6.1	×
	L7	4.8	4.8	4.7	4.8	×

(*continued*)

Table 5. (*continued*)

Classification	Dimension mark	MAD-1-pp(mm)	MAD-2-pp(mm)	MAD-3-pp(mm)	MAD-2-e(mm)	MAE
Width	W1	5.2	5.1	5.2	5.1	8
	W2	3.5	3.5	3.5	3.5	8
	W3	3.6	3.5	3.5	3.5	7
	W4	4.2	4.1	4.1	4.1	7
Depth	D1	2.6	2	2	2	4
	D2	2.8	2.1	2.1	2.1	4
	D3	4.6	4	4	4	8
	D4	3.1	2.5	2.5	2.5	9
	D5	2.6	2.3	2.3	2.3	9
Circumference	C1	6	5.5	5.4	4.3	6
	C2	7.2	6	5.9	5.1	6
	C3	9.8	7.4	7.2	5.9	15
	C4	8.3	7.5	7.4	6.2	15
	C5	9.4	7.9	7.2	6.6	11
	C6	9.7	7.4	7.2	6.4	12
	C7	8.5	7.5	7.5	7	9
	C8	7.8	7.2	7.1	6.1	9
	C9	6.2	5.3	5.2	4.9	×
	C10	6.8	5.7	5.4	4.6	×
	C11	9.4	8.6	8.4	7.2	9
	C12	8.6	7.7	7.5	6.6	9
	C13	8.4	7.1	7	6.2	×
	C14	9.1	8.6	8.3	7.2	×
	C15	9.2	8.8	8.5	6.4	9
	C16	7.9	7.3	7.2	5.8	×

It can be seen from Table 5 that the MAD value of MAD-1-pp is similar to that of MAD-2-pp and MAD-3-pp in height, length and width dimensions. It is worth noting that MAD-2-pp and MAD-3-pp are smaller than MAD-1-pp in depth, circumference dimensions. The results show that multi view images reconstruction method is more effective than the single view image reconstruction method. In addition, by comparing the values of MAD-2-pp and MAD-3-pp, it is found that the mean absolute difference of two methods is similar in most dimensions, and only in a few dimensions, values of MAD-3-pp method are smaller than that of MAD-2-pp method. Therefore, experiments show that dual image can contain enough body shape information. Considering users experience and measurement accuracy, the number of images used in the final multi view strategy is $n = 2$. On the other hand, comparing the MAD value of MAD-2-pp with mad value of MAD-2-e, the application of dense elliptic model algorithm in curve dimension (L4, L5) and circumference dimension reduces the measurement error. The results show

that our dense ellipse model algorithm can get smaller error than the point-to-point linear distance accumulation method.

In the process of measurement, the absolute difference of a dimension larger than MAE is inevitable, which is regarded as an abnormal value. In this paper, PA value is used as an index to evaluate the stability of measurement method. The PA value calculation formula of the kth dimension is defined as follows,

$$PA_k = \left(\frac{s}{n}\right) \times 100 \tag{12}$$

Where n is the number of volunteers and s is the number of outliers. We calculated PA values of some dimensions of 100 volunteers obtained by our method and other methods, and drew a bar chart, as shown in Fig. 10. Through analysis, we found that the average PA value of all dimensions of our proposed method was 95%, Murtaza's [16] method is 93%, and Liu's [12] method is 94.2%. Therefore, compared with other methods, our measurement method is more stable and accurate.

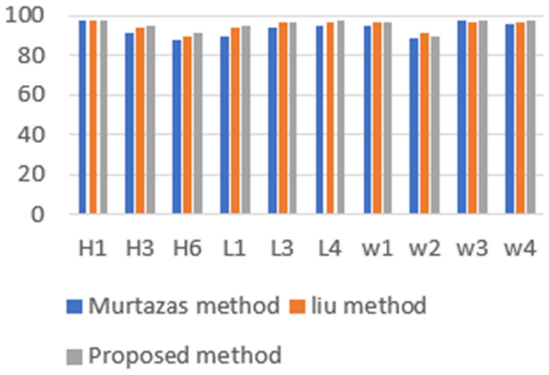

(a)

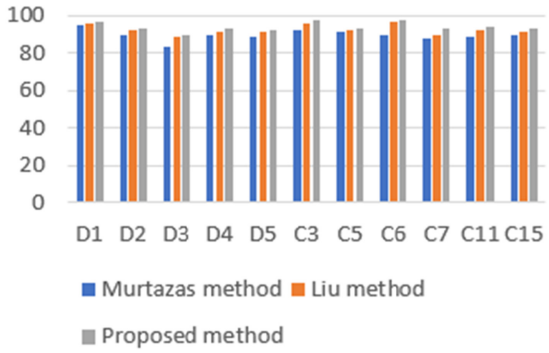

(b)

Fig. 10. The PA comparison of dimensions obtained by proposed method with other methods.

4 Conclusions

In this work, we present Mesh2Measure, an anthropometric dimensions measurement method based on 3D human body model. Compared with methods based on 2D human body contour, our method can extract more datum points and is more robust. The effect is almost the same as the manual measurement on a real human body. To make the reconstruction model more accurate, we fully extract and fuse human features of two view images. In addition, we propose a dense elliptic model method to calculate curve dimensions and closed circumference dimensions, which has higher fitting degree. The experimental results show that the proposed method is suitable for various body types, and the error of 38 main dimensions are smaller than that of existing methods. Therefore, anthropometric dimensions measured in our experiment can be used to assist medical health detection, sports, human body data analysis, garment customization and other fields. Future work can explore the anthropometric of a variety of postures and complex backgrounds, making the measurement more convenient and suitable for more situations.

Acknowledgments. This work was supported by National Natural Science Foundation of China (Grant Nos. 61873280, 61873281, 61972416), Taishan Scholarship (tsqn201812029), Major projects of the National Natural Science Foundation of China (Grant No. 41890851), Natural Science Foundation of Shandong Province (No. ZR2019MF012).

References

1. Baik, D., Sheng, J., Schlaffer, K., Friedenberg, F.K., Smith, M.S., Ehrlich, A.C.: Abdominal diameter index is a stronger predictor of prevalent Barrett's esophagus than BMI or waist-to-hip ratio. Diseases Esophagus **30**(9), 1–6 (2017)
2. De Koning, L., Merchant, A.T., Pogue, J., Anand, S. S.: Waist circumference and waist-to-hip ratio as predictors of cardiovascular events: meta-regression analysis of prospective studies. European Heart J. **28**(7), 850–856 (2007)
3. Dunk, N.M., Lalonde, J., Callaghan, J.P.: Implications for the use of postural analysis as a clinical diagnostic tool: reliability of quantifying upright standing spinal postures from photographic. J. Manipulative Physiol. Therapeutics **28**(6), 386–392 (2005)
4. Lemieux, I., Pascot, A., Couillard, C.: Hypertriglyceridemic waist: a marker of the atherogenic metabolic triad (hyperinsulinemia, hyperapo B, small, dense LDL)? Conf. 72nd Sci. Sessions Am. Heart Association (AHA) **102**(2), 179–184 (2000)
5. Chen, Y., Rennie, D., Cormier, Y.F., Dosman, J.: Waist circumference is associated with pulmonary function in normal-weight, overweight, and obese subjects. Am. J. Clinical Nutrit. **85**(1), 35–39 (2007)
6. Scott, I.A.: Thigh circumference and risk of heart disease and premature death. BMJ **339**(7723), 704–705 (2009)
7. Smith, D.A., et al.: Abdominal diameter index: a more powerful anthropometric measure for prevalent coronary heart disease risk in adult males. Diabetes Obesity Metabol. **7**(4), 370–380 (2005)
8. Heitmann, B.L., Frederiksen, P., Lissner, L.: Hip circumference and cardiovascular morbidity and mortality in men and women. Obesity Res. **12**(3), 482–487 (2004)
9. Debette, S., Leone, N., Courbon, D., et al.: Calf circumference is inversely associated with carotid plaques. Stroke **39**(11), 2958–2965 (2008)

10. Park, J.S., Cho, M.H., Ahn, C.W., et al.: The association of insulin resistance and carotid atherosclerosis with thigh and calf circumference in patients with type 2 diabetes. Cardiovasc. Diabetol. **11**(1), 62 (2012)
11. Lu, J.M., Twu, L.J., Wang, M.J.J.: Constructing 3D human model from front and side images. Expert Syst. Appl. **39**(5), 5012–5018 (2012)
12. Wang, X., Liu, B., Dong, Y., et al.: Anthropometric landmarks extraction and dimensions measurement based on ResNet. Symmetry **12**(12), 1997 (2020)
13. Xiao, Q.I., Zhongping, J.I.: Size measurement and fitting based on 3D human body model. College Comput. Sci. Eng. **643**(7), 76–83 (2019)
14. Wang, J., Jin, X.: three dimensional body measurement based on cnns and body silhouette. Master Thesis Zhejiang Univ. (2018)
15. Xu, L., Wu, X.: Research on the automatic measurement of 3D model of human body. Master Thesis Harbin Inst.Technol. (2019)
16. Aslam, M., Rajbdad, F., Khattak, S., Azmat, S.: Automatic measurement of anthropometric dimensions using frontal and lateral silhouettes. IET Comput. Vision **11**(6), 434–447 (2017)
17. Loper, M., Mahmood, N., Romero, J., et al.: SMPL: a skinned multi-person linear model. ACM Trans. Graphics **34**(6), 248 (2015)
18. Xiao, Y., Zhang, D.: Design and development of a garment and human body measurement system based on photography. Master Thesis Zhejiang Univ. (2019)
19. Kanazawa, A., Black, M.J., Jacobs, D. W., Malik, J.: End-to-end recovery of human shape and pose. IEEE Conf. Comput. Vision Pattern Recogn (CVPR) (2018)
20. Pavlakos, G., Zhu, L., Zhou, X., Daniilidis, K..: Learning to Estimate 3D Human Pose and Shape from a Single Color Image. In: The European Conference on Computer Vision and Pattern Recognition (CVPR), (2018)
21. Kolotouros, N., Pavlakos, G., Black, M.J., Daniilidis, K.: Learning to reconstruct 3D human pose and shape via model-fitting in the loop. In: International Conference on Computer Vision (ICCV), pp. 2252-2261 (2019)
22. Gabeur, V., Franco, J.S., Martin, X., Schmid, C., Rogez, G.: Moulding humans: non-parametric 3D human shape estimation from single images. In: IEEE/CVF International Conference on Computer Vision (ICCV), pp. 2232-2241 (2019)
23. Choi, H., Moon, G., Lee, K.M.: Pose2Mesh: Graph Convolutional Network for 3D Human Pose and Mesh Recovery from a 2D Human Pose. In: Vedaldi, A., Bischof, H., Brox, T., Frahm, J.-M. (eds.) ECCV 2020. LNCS, vol. 12352, pp. 769–787. Springer, Cham (2020). https://doi.org/10.1007/978-3-030-58571-6_45
24. Kolotouros, N., Pavlakos, G., Black, M.J., Daniilidis, K.: Convolutional mesh regression for single-image human shape reconstruction. In: The IEEE Conference on Computer Vision and Pattern Recognition (CVPR), pp. 4501–4510 (2019)
25. Moon, G., Lee, K.M.: I2L-MeshNet: Image-to-Lixel Prediction Network for Accurate 3D Human Pose and Mesh Estimation from a Single RGB Image. In: Vedaldi, A., Bischof, H., Brox, T., Frahm, J.-M. (eds.) ECCV 2020. LNCS, vol. 12352, pp. 752–768. Springer, Cham (2020). https://doi.org/10.1007/978-3-030-58571-6_44
26. Moon, G., Lee, K.M.: Pose2Pose: 3D positional pose-guided 3D rotational pose prediction for expressive 3D human pose and mesh estimation. In: The IEEE Conference on Computer Vision and Pattern Recognition (CVPR) (2020)
27. He, K., Zhang, X., Ren, S., Sun, J.: Deep residual learning for image recognition. In: IEEE Conference on Computer Vision and Pattern Recognition (CVPR), pp. 27–30 (2016)
28. Kipf, T.N., Welling, M.: Semi-supervised classification with graph convolutional networks. In: The International Conference on Learning Representations (ICLR) (2017)
29. GB/T 16160–2017: Anthropometric Definitions and Methods for Garment; Standards Press of China: Beijing (2017)

30. GB/T 38131–2019: Acquisition Method of Datum Points for Clothing Anthropometry; Standards Press of China: Beijing, China (2019)
31. Dibra, E., Jain, H., Oztireli, C., Ziegler, R., Gross, M.: HS-nets: estimating human body shape from silhouettes with convolutional neural networks. In: Fourth International Conference on 3D Vision (3DV), pp. 108–117 (2016)
32. Technicolor, T., Related, S., Technicolor, T.: ImageNet Classification with Deep Convolutional Neural Networks. Curran Associates Inc, NIPS (2012)
33. Simonyan, K., Zisserman, A.: Very deep convolutional networks for large-scale image recognition. Comput. Sci. (2014)
34. Szegedy, C., Liu, W., Jia, Y.: Going deeper with convolutions. In: Proceedings of the IEEE Conference on Computer Vision and Pattern Recognition, (pp. 1-9) (2014)
35. Bogo, F., Kanazawa, A., Lassner, C., Gehler, P., Romero, J., Black, M.J.: Keep It SMPL: Automatic Estimation of 3D Human Pose and Shape from a Single Image. In: Leibe, B., Matas, J., Sebe, N., Welling, M. (eds.) ECCV 2016. LNCS, vol. 9909, pp. 561–578. Springer, Cham (2016). https://doi.org/10.1007/978-3-319-46454-1_34
36. Lassner, C., Romero, J., Kiefel, M., Bogo, F., Black, M.J., Gehler, P.V.: Unite the people: closing the loop between 3D and 2D human representations. In: CVPR (2017)
37. Omran, M., Lassner, C., Pons-Moll, G., Gehler, P., Schiele, B.: Neural body fitting: unifying deep learning and model based human pose and shape estimation. In: 3DV (2018)
38. Zhou, X., Zhu, M., Pavlakos, G., Leonardos, S., Derpanis, K.G., Daniilidis, K.: Monocap: monocular human motion capture using a CNN coupled with a geometric prior. PAMI **41**(4), 901–914 (2019)